A chiral porous organic polymer as a heterogeneous ligand for enantioselective Pd-catalyzed C(sp3)-H functionalization

Bennedsen, Niklas Rosendal; Kramer, Søren; Kegnæs, Søren

Published in:
Catalysis Science and Technology

Link to article, DOI:
10.1039/d0cy01326a

Publication date:
2020

Document Version
Peer reviewed version

Catalysis Science & Technology

Accepted Manuscript

This article can be cited before page numbers have been issued, to do this please use: N. R. Bennedsen, S. Kramer and S. Kegnæs, *Catal. Sci. Technol.*, 2020, DOI: 10.1039/D0CY01326A.

ROYAL SOCIETY OF CHEMISTRY

rsc.li/catalysis

View Article Online
DOI: 10.1039/D0CY01326A

ARTICLE

A Chiral Porous Organic Polymer as Heterogeneous Ligand for Enantioselective Pd-Catalyzed C(sp^3)–H Functionalization

Received 00th January 20xx,
Accepted 00th January 20xx

DOI: 10.1039/x0xx00000x

Niklas R. Bennedsen[a], Søren Kramer*[a], and Søren Kegnæs*[a]

Catalytic enantioselective C(sp^3)–H functionalization remains a difficult task, even more so using heterogeneous catalysts. Here, we report the first example of enantioselective C(sp^3)–H functionalization using a chiral porous organic polymer as the heterogeneous catalyst. The catalyst consists of a polystyrene-incorporated chiral phosphoramidite coordinated to palladium, and it provides up to 86% ee for the challenging enantioselective C(sp^3)–H functionalization of a range of 3-arylpropanamides. The swelling properties of the catalyst allow for quasi-homogeneous behavior in the reaction mixture while still enabling easy catalyst separation from the reaction medium and reuse. Thorough characterization of the fresh porous organic polymer and recycled catalyst material by ^{31}P CP/MAS NMR, ^{13}C–^{1}H CP/MAS NMR, X-ray diffraction, TEM, STEM, EDX-SEM, ICP, and XRF in combination with modifications to the reaction conditions for the recycled catalyst material reveals potential explanations for catalyst deactivation.

Introduction

Heterogeneous catalysis is generally preferred for industrial applications due to the inherent benefits of having the catalytic species separated from reactants and products, such as easier recovery of the catalyst for recycling or for removal of undesired transition-metal impurities.[1] These features can provide economic benefits and lead to more sustainable processes.[2] While heterogeneous catalysis is typically associated with high activity, the activity is often accompanied by poor selectivity in comparison to their homogeneous counterparts. This limitation prevents the implementation of heterogeneous catalysis in the fine-chemical industry where selectivity is essential, especially in the production of optically pure compounds such as pharmaceuticals, fragrances, and agrochemicals.[1e,3] Thus, the development of heterogeneous catalysts which provide high enantioselectivity is an important objective for adapting heterogeneous catalysis to fine-chemical production.

Porous organic polymers (POPs) are promising materials for the development of new and highly selective heterogeneous catalysts.[4] Especially their functional freedom sets them aside from other heterogeneous catalyst types such as covalent organic frameworks, metal organic frameworks, aluminosilicates, and metaloxides, which all have compositional restraints and/or requires crystallinity.[5] In contrast, POPs have a high tolerance for different functional groups, and the covalent incorporation of a variety of different ligands into the polymer backbone is straightforward. Notably, polystyrene-based POPs swell in appropriate solvents which can provide a quasi-homogeneous environment around the ligand-metal center.[6] This feature allows the POP-based catalysts to mimic the selectivity of homogeneous systems while maintaining the traditional advantages of heterogeneous catalyst materials such as easy catalyst separation.[7] Several ligands typically used in transition-metal catalysis have been incorporated into polystyrene-based POPs including PPh_3, BINAP, DPPBz, biphephos, Xantphos, and phosphoramidite.[8] Yet, the applications of these catalyst materials have predominantly focused on high-pressure reactions involving gases, especially hydrogenation and hydroformylation.

Catalytic enantioselective C(sp^3)–H functionalization is a challenging reaction class, which nonetheless holds great potential for sustainable synthesis of fine chemicals.[9] To date, there are no examples of enantioselective C(sp^3)–H functionalization using a chiral POP catalyst. A few examples of racemic or non-stereogenic C(sp^3)–H functionalization with achiral POP catalysts have been reported.[8g,10] Notably, Jones and Yu *et al.* published a substrate-directed C(sp^3)–H arylation catalyzed by a palladium-aminopyridine-POP.[10f] In general, the C(sp^3)–H functionalization products were obtained in good yields. Furthermore, their catalyst system represents an uncommon example of metal and ligand recycling in a C(sp^3)–H functionalization reaction, albeit significant deactivation was observed in the third consecutive run even upon addition of fresh palladium complex. No investigation of deactivation pathways was performed, and no examples of enantioselective C(sp^3)–H functionalization were included.

Here, we report the first enantioselective C(sp^3)–H functionalization using a chiral POP catalyst. The catalyst is comprised of a polystyrene-incorporated chiral phosphoramidite coordinated to palladium, and it provides up to 86% ee for the challenging enantioselective C(sp^3)–H

[a] Department of Chemistry, Technical University of Denmark, 2800 Kgs. Lyngby, Denmark. Email: sokr@kemi.dtu.dk (S. Kramer), skk@kemi.dtu.dk (S. Kegnæs)

†Electronic Supplementary Information (ESI) available: See DOI: 10.1039/x0xx00000x

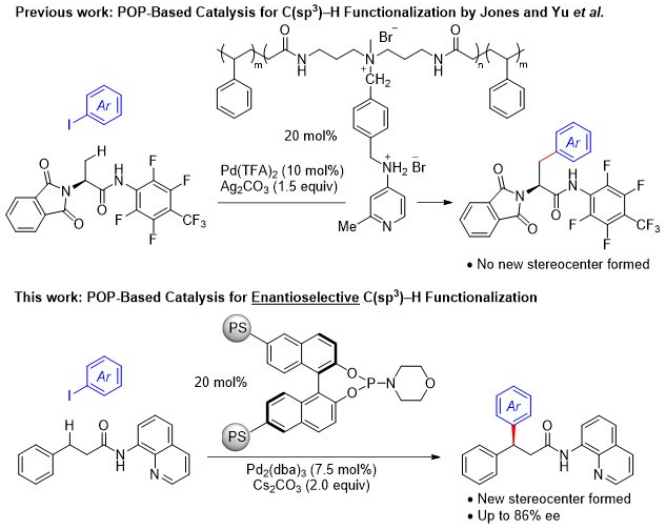

Scheme 1 C(sp³)-H Functionalization by POP-Based Catalysts.

arylation of 3-arylpropanamides. With the addition of fresh palladium, the chiral POP can be reused albeit displaying a slow loss of enantioselectivity upon multiple reuses. Thorough characterization of the recycled catalyst material was performed leading to the first insights into the deactivation pathways for POP catalysts used for C(sp³)–H functionalization.

Results and Discussion

Combining our interests in asymmetric catalysis, heterogeneous catalysis, and C(sp³)–H functionalization, we set out to develop the first heterogeneous enantioselective C(sp³)–H functionalization catalyzed by a chiral POP.[4d,11] We targeted the synthesis of a polystyrene-based phosphoramidite-containing POP inspired by a recent publication on the homogeneous enantioselective C(sp³)–H arylation of 3-arylpropanamides.[9n] Starting from enantiopure (*R*)-BINOL, the vinylated enantiopure phosphoramidites were obtained in three steps (Scheme 2a). Initial bromination of (*R*)-BINOL proceeded selectively in the 4,4'-positions affording a high yield of the dibrominated (*R*)-BINOL **1**. Subsequent vinylation by a palladium-catalyzed Suzuki cross-coupling reaction with potassium vinyltrifluoroborate led to clean formation of the divinylated (*R*)-BINOL **2**. From this intermediate, the morpholine phosphoramidite **3** was accessed by treatment with phosphor trichloride in the presence of N-methyl-2-pyrrolidone (NMP) followed by addition of morpholine. The dimethylamine phosphoramidite **4** was synthesized from intermediate **2** by the addition of $P(NMe_2)_3$. Finally, the phosphoramidite ligands were incorporated into polystyrene polymers by AIBN-initiated radical polymerization in THF in the presence of styrene (50 equiv) and divinylbenzene (1.06 equiv) (Scheme 2b).[8f,8h] The phosphoramidite-containing POPs were obtained as fine powders (Figure S4).

With the two chiral phosphoramidite-POPs in hand, we tested them in the palladium-catalyzed enantioselective C(sp³)–H arylation of a 3-phenylpropanamide (Table 1). Encouragingly, the use of either of the chiral-POPs led to formation of the desired product with significant levels of enantioselectivity. Nonetheless, with 70% yield and 86% ee, the morpholine-phosphoramidite-POP was clearly superior to the dimethyl-phosphoramidite. We named this morpholine-phosphoramidite-POP with a 1:50 ratio between ligand and styrene "(*R*)-P-amidite-POP".

To further fine-tune the catalyst, we investigated the influence of ligand density in the polymer. Accordingly, a series of morpholine-phosphoramidite-POPs were synthesized by varying the ratio between styrene and phosphoramidite. When tested in the enantioselective C(sp³)–H functionalization, it was clear that increasing the ligand density in the POP decreases the catalytic activity (Table 2). The increased ligand density also leads to larger average particle sizes, likely due to the crosslinking effect of the ligand (Figure S4).

Having demonstrated proof-of-concept that chiral POP-based catalysts can facilitate enantioselective C(sp³)–H functionalization, thorough characterization was carried out of

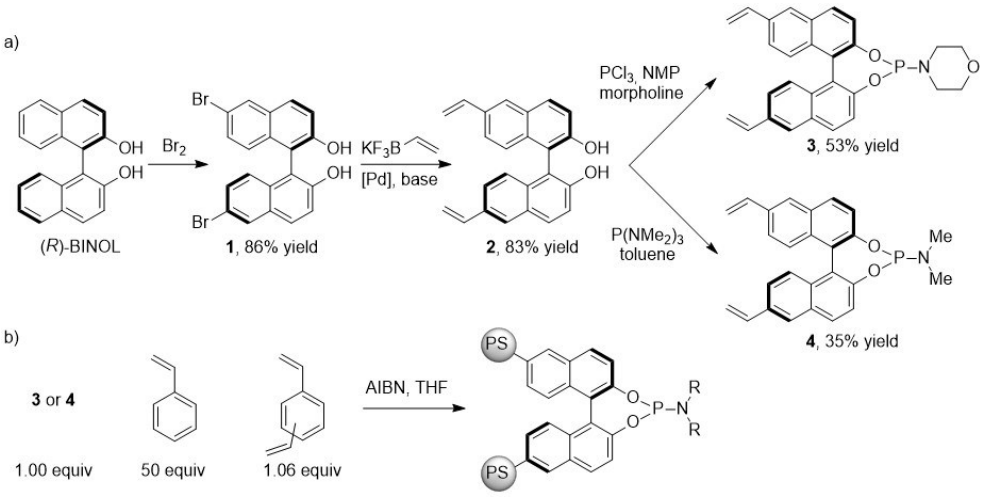

Scheme 2 (a) Synthesis of Vinylated Phosphoramidites and (b) Synthesis of POP containing Chiral Phosphoramidites.

the best-performing catalyst (the morpholine-phosphoramidite-POP with a 1:50 ratio between ligand and

Table 1 Catalytic Performance of Two Different POPs in the C(sp³)–H Functionalization

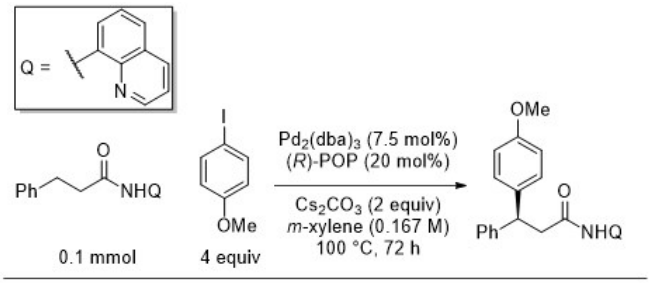

Entry	Ligand	Conv.[a] (%)	Yield[a] (%)	ee[b] (%)
1	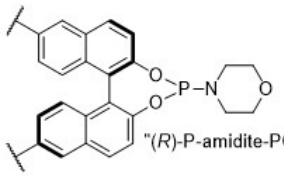 "(*R*)-P-amidite-POP"	70	70	86
2	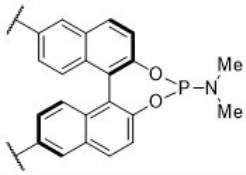	100	49	72

of a 3-Arylpropanamide.

[a]Conversion and yield determined by ^{1}H-NMR using an internal standard. [b]Enantiomeric excess determined by chiral HPLC.

styrene which is abbreviated (*R*)-P-amidite-POP). Thermal gravimetric analysis demonstrated good thermal stability for the (*R*)-P-amidite-POP with no loss of mass in air up to over 300 °C (Figure 1). Scanning electron microscopy (SEM) revealed the morphology of the synthesized POP as spherical particles in a broad size distribution from 100 nm up to 3 µm (Figure S5). When examined by N_2-physisorption, the dry (*R*)-P-amidite-POP displayed a low pore volume (0.049 cm³/g) and a low surface area (24 m²/g) (Figure S6). These features underscore the importance of the swelling properties for providing the necessary access to the active sites. Indeed, the synthesized (*R*)-P-amidite-POP swells to the point where goes into solution in range of different solvents (Figure 2a). The clear solutions

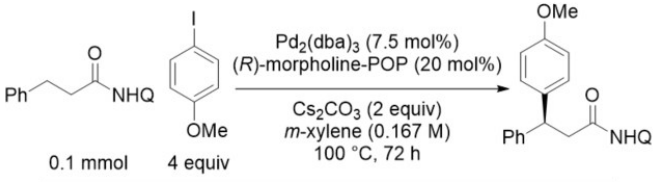

Entry	Ligand:Styrene ratio	Conv.[a] (%)	Yield[a] (%)
1	1:50 ("(*R*)-P-amidite-POP")	70	70
2	1:25	30	27
3	1:15	29	23
4	1:5	20	16

obtained with *m*-xylene, toluene, benzene, dioxane, and THF indicate the likeliness of a quasi-homogeneous environment at

b)

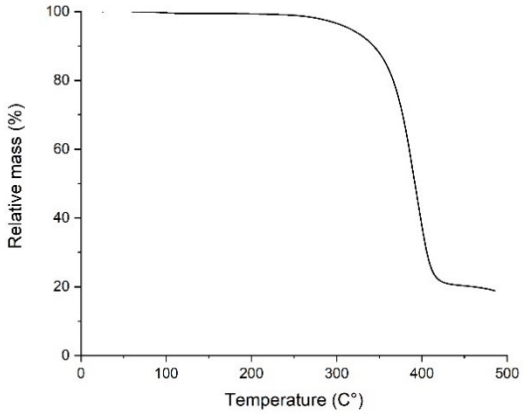

Figure 1 Thermal gravimetric analysis of (*R*)-P-amidite-POP with a heating ramp of 10 °C/min up to 500 °C in air.

Table 2 The Influence on the Catalytic Performance of Varying Ligand/Styrene Ratios in the Morpholine-Phosphoramide POP.

[a]Conversion and yield determined by ^{1}H-NMR using an internal standard.

the ligand sites in these solvents (Figure 2b). This suggestion was further supported by the observation of a fairly sharp signal in the liquid phase ^{31}P NMR spectrum of (*R*)-P-amidite-POP in d_8-toluene. In contrast, the (*R*)-P-amidite-POP does not swell in hexane, thus precipitation by addition of hexane allows for easy catalyst separation. However, the extensive swelling of (*R*)-P-amidite-POP made filtration experiments impossible without addition of an anti-solvent such as hexane.

To examine the (*R*)-P-amidite-POP in dry form, ^{31}P CP/MAS NMR was performed (Figure 3, top). The spectrum shows that the phosphoramidite is preserved with a characteristic chemical shift at 143 ppm, which is very close to 144 ppm observed for morpholine-phosphoramidite **3**. A small signal at 9 ppm indicates that a small fraction of phosphoramidites have been oxidized.[9n] ^{13}C–^{1}H CP/MAS NMR was also performed on the (*R*)-P-amidite-POP (Figure 3, bottom). The peak observed at 67 ppm

a)

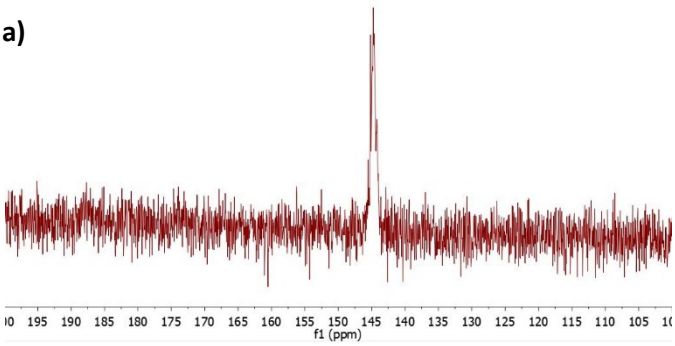

Figure 2 (a) Picture showing the appearance of (*R*)-P-amidite-POP in a range of solvents. (b) Liquid phase ^{31}P NMR of (*R*)-P-amidite-POP in d_8-toluene.

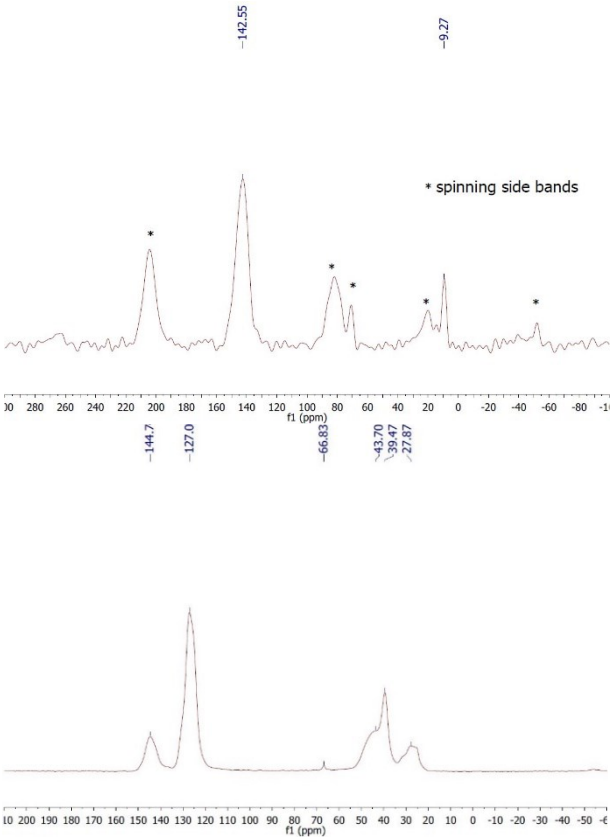

Figure 3 (Top) ^{31}P CP/MAS NMR of the (*R*)-P-amidite-POP at a spinning frequency of 15 kHz where the spinning side bands are indicated. (Bottom) ^{13}C–^{1}H CP/MAS NMR of the POP at a spinning frequency of 15 kHz.

corresponds to the morpholine moiety in the polymer-bound phosphoramidite. The remaining peaks are in good correlation with previously reported polystyrene backbones in POPs.[8g,8h] Having confirmed the nature and characteristics of the chiral POP-based catalyst material, we returned to the evaluation of the catalytic performance. A series of variations to the reaction conditions and control experiments were performed (Table 3). Under the optimized reaction conditions, the reaction utilizes 7.5 mol% $Pd_2(dba)_3$ as palladium source, 20 mol% (*R*)-P-amidite-POP, 4 equivalents aryl iodide, and 2 equivalents Cs_2CO_3 in m-xylene at 100 °C for 72 hours (entry 1).[12] In the absence of (*R*)-P-amidite-POP the product is still formed but only as racemate, indicating the potential risk of a racemic background reaction if the amount of palladium exceeds that of the ligand (entry 2). Shortening the reaction time led to a small decrease in yield while the addition of more (*R*)-P-amidite-POP inhibited product formation (entries 3-4). Lowering the palladium loading provided a decrease in yield (entry 5). Other palladium sources led to lower enantioselectivities (entries 6-7). Finally, palladium nanoparticles were found inactive as catalysts for the reaction (entry 8).

Next, the generality of the enantioselective C(sp^3)–H functionalization using the chiral POP-based catalyst was examined (Table 4). The influence of the 3-arylpropanamide was investigated first. A substrate bearing a *meta*-methyl substituent afforded high yield and enantioselectivity, identical to the phenyl substrate (entries 1-2). The introduction of a *meta*-methoxy group afforded a good yield but with a small decrease in enantioselectivity (entry 3). Albeit reacting more sluggishly, fluorides in the *meta*- or *para*-position also led to good enantioselectivities (entries 4-5). Finally, the bulkier 3,5-dimethyl-substituted substrate provided product in good yield and enantioselectivity (entry 6). The influence of the electronic properties of the aryl iodide was also investigated. While the 4-

Table 3 Influence of Various Reaction Parameters on the Reaction Outcome for the Enantioselective C(sp^3)–H Functionalization Utilizing a Chiral POP-Based Catalyst.

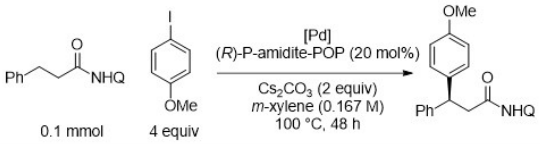

Entry	[Pd] (equiv)	Other modifications	Conv. (%)[a]	Yield. (%)[a]	ee (%)[b]
1	$Pd_2(dba)_3$(0.075)	72 h	70	70	86
2	$Pd_2(dba)_3$(0.075)	no (*R*)-P-amidite-POP, 72 h	66	51	0
3	$Pd_2(dba)_3$(0.075)	-	63	60	87
4	$Pd_2(dba)_3$(0.075)	30 mol% (*R*)-P-amidite-POP	45	38	75
5	$Pd_2(dba)_3$(0.05)	-	68	65	69
6	$Pd_2(dba)_3$•$CHCl_3$ (0.05)	-	78	66	61
7	$Pd(dba)_2$ (0.10)	-	53	46	84
8	Pd/C (0.15)	no (*R*)-P-amidite-POP, 72 h	86	0	-

[a]Conversion and yield determined by ^{1}H-NMR using an internal standard. [b]Enantiomeric excess determined by chiral HPLC.

Table 4 Investigation of Substrate Scope for the Enantioselective C(sp^3)–H Functionalization.

[a]Conversion and yield determined by ^{1}H-NMR using an internal standard.

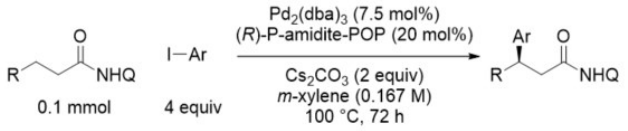

Entry	I—Ar	R	Yield (%)[a]	ee (%)[b]
1	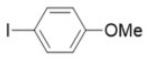		70	86
2	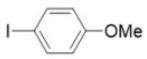		70	86
3	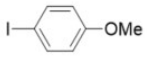		62	68
4	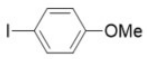		45	86
5	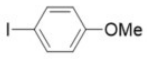	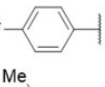	35	84
6	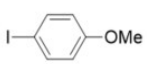		62	84
7	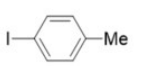		51	78
8	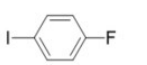		13	66

[b]Enantiomeric excess determined by chiral HPLC.

iodotoluene afforded the product with synthetically useful yield and ee, an electron-poor fluoride-substituted iodobenzene only afforded low yield (entries 7-8). Overall, the results indicate that the reaction provides the highest yields and enantioselectivities with 3-arylpropanamides bearing electron-neutral substituents and electron-rich aryl iodides.

Our tentative mechanistic hypothesis for the enantioselective C(sp^3)–H arylation is based on previous work by Chen et al.[9n] The catalytic cycle is initiated by oxidative addition of the aryl iodide to ligand-bound palladium(0). Subsequent coordination of deprotonated 3-arylpropanamide enables palladation of the C–H bond. Finally, reductive elimination affords the arylated product and regenerates palladium(0).

Given the heterogeneous aspects of the developed catalyst system, we were curious to explore the possibilities for catalyst recovery and recycling. While the (*R*)-P-amidite-POP swells extensively in m-xylene, it de-swells upon addition of an anti-solvent such as hexane (Figure 2a). Accordingly, hexane was added at the end of the reaction causing the catalyst material to solidify. Removal of the liquid phase easily separates the products and reactants from the catalyst material, which can then be recycled for a new reaction.

Initial recycling using the recovered solid as a source of chiral ligand and palladium under unmodified reaction conditions revealed a small decrease in enantioselectivity but a substantial decrease in catalytic activity (Table 5, entries 2-4). Inspired by the work by Jones and Yu *et al.*[10f] who showed that recycling beyond two runs was only feasible upon addition of new palladium source to each run, we also speculated if the overall deactivation in our reaction originated from either loss of or deactivation of the active palladium species rather than deterioration of the (*R*)-P-amidite-POP. Hence, recycling was attempted with $Pd_2(dba)_3$ added to each new run (entries 5-7). Now, the second run produced an increased yield while still affording good enantioselectivity, thus indicating successful reuse of the chiral POP material. Given the concomitant gradual decrease in enantioselectivity, we hypothesize that any excess of palladium in comparison to available chiral ligand sites leads to a competing racemic background reaction (Table 3, entry 2). Nonetheless, the results presented here illustrates the potential of POP-based ligands as a means for reuse of expensive chiral ligands.

In order to gain further insights into any changes to the (*R*)-P-amidite-POP arising during the reaction as well as potential origins of deactivation, we performed thorough characterization of the dried catalyst material recovered after the first run. By X-Ray diffraction, the presence of palladium nanoparticles and cesium iodide could be observed at 2θ = 40 and 2θ = 28, 39, and 49, respectively (Figure 4a). The presence of palladium nanoparticles and cesium iodide was also confirmed by electron microscopy (Figure 4b-c and Figure 5). The biggest particles (20-250 nm) were cesium iodide based on EDX analysis whereas palladium was present as small nanoparticles (2-4 nm) evenly distributed throughout the whole sample (Figure 5). Accordingly, the formation of inactive palladium nanoparticles (see Table 3, entry 8) under the reaction conditions is likely a major contributor to the observed decrease in activity in the absence of additional $Pd_2(dba)_3$. In contrast, ICP analysis of the extracted liquid phase showed that it contained less than 0.01% of the originally added palladium, thus indicating that leaching is not contributor to the deactivation (Figure S1). The same conclusion was reached with XRF measurements (Figure S2). Examining the liquid phase in ^{31}P-NMR did not show any phosphorus-containing species which indicates that all the ligand entities are incorporated into the POP. Accordingly, enantioselective product formation cannot arise from homogeneous species (Figure S3).

Table 5 Reuse of the (*R*)-P-amidite-POP for Enantioselective C(sp^3)–H Functionalization.

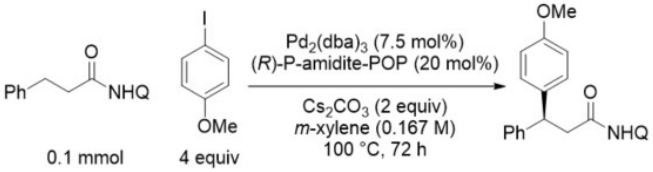

Entry	Run	Modifications	Conv. (%)[a]	Yield (%)[a]	ee (%)[b]
1	1	-	70	70	86
2	2	-	32	32	73
3	3	-	15	10	65
4	4	-	0	0	-
5	2	Add. of fresh Pd	100	99	74
6	3	Add. of fresh Pd	100	91	62
7	4	Add. of fresh Pd	100	73	54

Fresh Cs_2CO_3 (2 equiv) was added to each new cycle. [a]Conversion and yield determined by ^{1}H-NMR using an internal standard. [b]Enantiomeric excess determined by chiral HPLC.

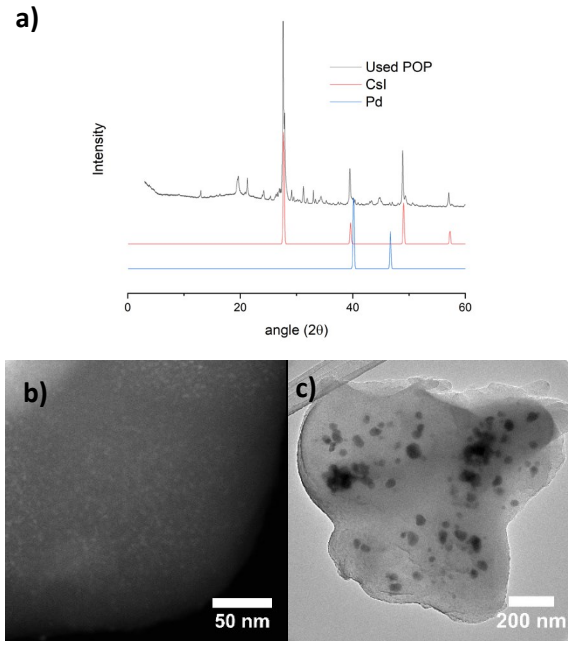

Figure 4 Characterization of the used (*R*)-P-amidite-POP catalyst. a) XRD diffractogram of the used (*R*)-P-amidite-POP. b) Dark field STEM image of the used (*R*)-P-amidite-POP. c) Bright field TEM image of the used (*R*)-P-amidite-POP.

View Article Online
DOI: 10.1039/D0CY01326A

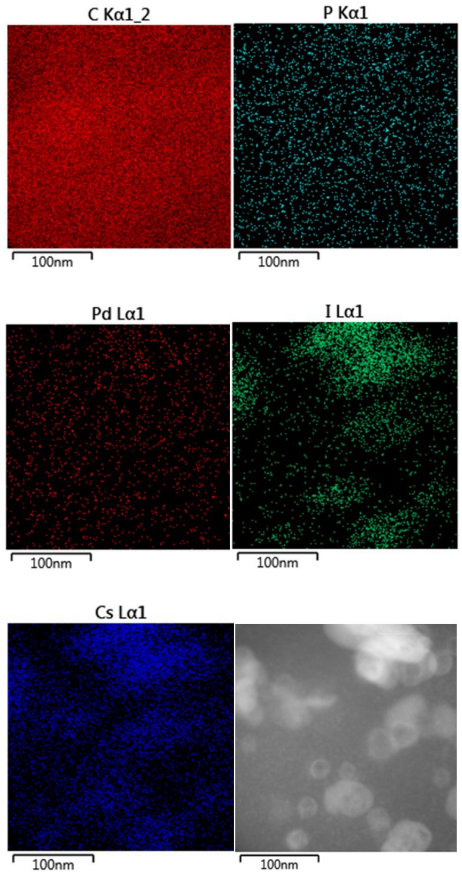

Figure 5 EDX analysis of the used (*R*)-P-amidite-POP showing the presence of CsI particles as well as palladium and phosphor throughout the whole sample.

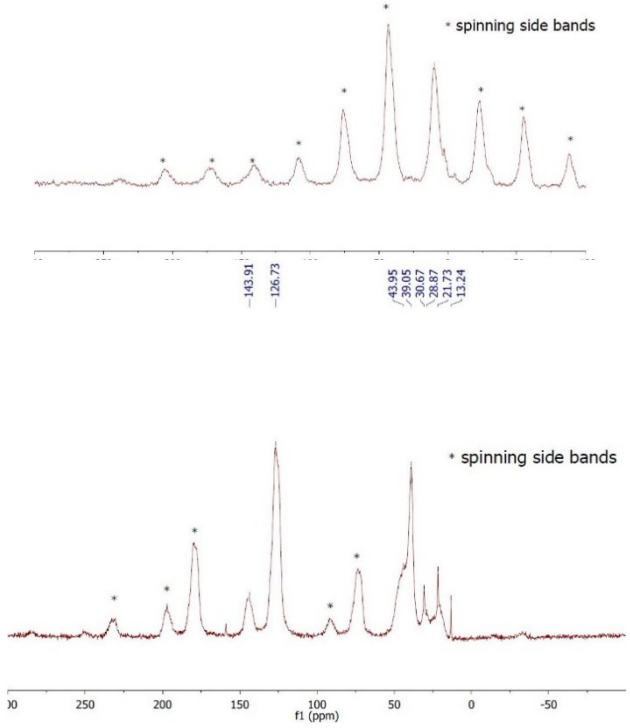

Figure 6 (Left) ^{31}P CP/MAS NMR of the used (*R*)-P-amidite-POP at a spinning frequency of 8 kHz where the spinning side bands are indicated with asterisks. (Right) ^{13}C–^{1}H CP/MAS NMR of the used (*R*)-P-amidite-POP at a spinning frequency of 8 kHz showing the polystyrene polymer and the presence of hexane at 30.7, 21.7 and 13.2 ppm. Spinning side bands are indicated with asterisks.

Even distribution of phosphorus in the recycled catalyst material, observed by EDX, shows that the ligand is still present in the polymer material (Figure 5). Nonetheless, to obtain more detailed information, ^{31}P CP/MAS and ^{13}C–^{1}H CP/MAS NMR spectra of the recovered catalyst material were recorded (Figure 6). Surprisingly, the ^{31}P CP/MAS NMR spectrum shows the complete disappearance of the phosphoramidite moiety with concomitant appearance of a major signal 10 ppm. This newly formed phosphor species correlates to the oxidized form of the phosphoramidite, $(RO)_2P(O)NR_2$, thus suggesting that the phosphoramidite moiety is not stable under the reaction conditions or that it reacts with air during the recovery of the catalyst.[9n] Fortunately, the recycling experiments indicate that the oxidized form of the phosphoramidite is also able to induce good levels of enantioselectivity in the C(sp^3)–H functionalization of 3-arylpropanamides (Table 5, entries 2 and 5). The ^{13}C–^{1}H CP/MAS NMR spectrum still shows the presence of the polystyrene backbone and some sharp signals from hexane trapped inside the POP at 30.7, 21.7 and 13.2 ppm. Finally, SEM images revealed a morphology change from the fresh to the recycled POP, however, this is expected as different solvent combinations were used to solidify the catalyst material (Figure S7).

Conclusion

In summary, we have reported the first example of enantioselective C(sp^3)–H functionalization which utilize a chiral POP as the heterogeneous catalyst. The catalyst consists of a polystyrene-incorporated chiral phosphoramidite coordinated to palladium. The swelling properties of the POP enables a quasi-homogeneous environment at the ligand sites, while still allowing for easy catalyst separation upon addition of an anti-solvent. The catalytic system provides up to 86% ee for the challenging enantioselective C(sp^3)–H coupling reaction of several of 3-arylpropanamides and aryl iodides. The chiral POP can be reused, if new palladium source is added, albeit with a gradual loss of enantioselectivity. The need for additional palladium is predominantly due to the formation of palladium nanoparticles, while the gradual loss of enantioselectivity likely originates from the racemic background reaction catalyzed by excess palladium. Solid-state NMR spectroscopy clearly shows the successful incorporation of the phosphoramidite into the polystyrene-POP; however, complete ligand oxidation was observed after subjection to the reaction conditions. Nonetheless, the oxidized ligand can still induce good levels of enantioselectivity. Overall, these observations provide the first

insights into deactivation pathways for heterogeneous C(sp^3)–H functionalization by POP-catalysts. Despite the observed deactivation pathways, the chiral-POP catalyst system presented here demonstrate the potential for future development of the powerful concept: ligand recycling in enantioselective C(sp^3)–H functionalization. We are currently developing more robust recyclable chiral POP-catalysts for enantioselective catalysis.

Conflicts of interest

There are no conflicts to declare.

Acknowledgements

The authors thank Dr. Kasper Enemark-Rasmussen at the DTU NMR center supported by the Villum foundation for aid with solid-state NMR. We also thank David B. Christensen for aid with TEM and STEM, Dr. Farnoosh Goodarzi for aid with SEM, and Karoline H. Rasmussen for synthesis of a few substrates. The authors are grateful for funding from the Independent Research Fund Denmark (grant no. 6111-00237), from Villum fonden (Grant No. 13158), and from Haldor Topsøe A/S. S. Kramer is deeply appreciative of generous financial support from the Lundbeck Foundation (Grant No. R250-2017-1292) and the Technical University of Denmark.

Notes and references

1 a) C. Copéret, M. Chabanas, R. Saint-Arroman, J.-M. Basset, *Angew. Chem. Int. Ed.* 2003, **42**, 157-181, (b) J. Thomas, R. Raja, D. Lewis, *Angew. Chem. Int. Ed.* 2005, **44**, 6465-6482, (c) D. Astruc, F. Lu, J. Aranzaes, *Angew. Chem. Int. Ed.* 2005, **44**, 7852-7872, (d) C. Witham, W. Huang, C.-K. Tsung, G. Somorjai, F. Toste, *Nat. Chem.* 2010, **2**, 36-41, (e) J. Magano, J. Dunetz, *Chem. Rev.* 2011, **111**, 2177-2255, (f) G. Rupprechter, *Nat. Chem.* 2017, **9**, 833-834.

2 (a) P. Anastas, L. Bartlett, M. Kirchhoff, T. Williamson, *Catalysis Today*, 2000, **55**, 11-22, (b) P. Anastas, M. Kirchhoff, T. Williamson, *Appl. Catal. A.* 2001, **221**, 3-13, (c) J. Clark, *Pure Appl. Chem.* 2001, **73**, 103-111, (d) P. Anastas, J. Zimmerman, *Green Chem*. 2019, **21**, 6545-6566.

3 (a) M. Gruttadauria, F. Giacalone, *Catalytic Methods in Asymmetric Synthesis*, 2011, John Wiley & Sons. ISBN: 978-0-470-64136-1, (b) C. Busacca, D. Fandrick, J. Song, C. Senanayake, *Adv. Synth. Catal.* 2011, **353**, 1825-1864.

4 (a) P. Kaur, J. Hupp, S. Nguyen, *ACS Catal.* 2011, **1**, 819-835, (b) Y. Zhang, N. Riduan, *Chem. Soc. Rev.* 2012, **41**, 2083-2094, (c) Q. Sun, Z. Dai, X. Meng, F.-S. Xiao, *Chem. Soc. Rev.* 2015, **44**, 6018-6034, (d) S. Kramer, N. Bennedsen, S. Kegnæs, *ACS Catal.* 2018, **8**, 6961-6982.

5 (a) Y. Ma, W. Tong, H. Zhou, S. Suib, *Micropor. Mesopor. Mat.*, 2000, **37**, 243-252, (b) J. Pérez-Ramirez, C. Christensen, K. Egeblad, C. Christensen, J. Groen, *Chem. Soc. Rev.* 2008, **37**, 2530-2542, (c) J. Lee, O. Farha, J. Roberts, K. Scheidt, S. Nguyen, J. Hupp, *Chem. Soc. Rev.* 2009, **38**, 1450-1459, (d) S.-Y. Ding, W. Wang, *Chem. Soc. Rev.* 2013, **42**, 548-568, (e) Y. Wang, H. Arandiyan, J. Scott, A. Bagheri, H. Dai, R. Amal, *J. Mater. Chem. A.* 2017, **5**, 8825-8846, (f) J. Zhang, X. Han, X. Wu, Y. Liu, Y. Cui, *J. Am. Chem. Soc.* 2017, **139**, 8277-8285, (g) F. Goodarzi, L. Kang, F. Wang, F. Joensen, S. Kegnæs, J. Mielby, *ChemCatChem* 2018, **10**, 1566-1570, (h) M. Samantaray, E. Pump, A. Bendjeriou-Sedjerari, V. D'Ella, J. Pelletier, P. Guidotti, J.-M. Basset, *Chem. Soc. Rev.* 2018, **47**, 8403-8437, (i) A. Dhakshinamoorthy, A. Asiri, H. Garcia, *ACS Catal.* 2019, **9**, 1081-1102, (j) L. Gonçalves, D. Christensen, M. Meledina, L. Salonen, D. Petrovykh, J. Sousa, O. Soares, M. Pereira, S. Kegnæs, Y. Kolen'ko, *Catal. Sci. Technol.* 2020, **10**, 1991-1995.

6 Q. Sun, Z. Dai, X. Liu, N. Sheng, F. Deng, X. Meng, S. Xiao, *J. Am. Chem. Soc.* 2015, **137**, 5204-5209.

7 (a) P. Hodge, *Chem. Soc. Rev.* 1997, **26**, 417-424, (b) W. Wang, A. Zheng, P. Zhao, C. Xia, F. Li, *ACS Catal.* 2014, **4**, 321−327, (c) X. Wang, S. Lu, J. Li, Y. Liu, C. Li, *Catal. Sci. Technol*. 2015, **5**, 2585−2589, (d) Z. Dai, Q. Sun, X. Liu, C. Bian, Q. Wu, S. Pan, L. Wang, X. Meng, F. Deng, F.-S. Xiao, *J. Catal*. 2016, **338**, 202−209, (e) Y. Xu, T. Wang, Z. He, M. Zhou, W. Yu, B. Shi, K. Huang, *Appl. Catal. A*, 2017, **541**, 112−119, (f) R. Cai, X. Ye, Q. Sun, Q. He, Y. He, S. Ma, X. Shi, *ACS Catal.* 2017, **7**, 1087−1092.

8 (a) T. Iwai, T. Harada, K. Hara, M. Sawamura, *Angew. Chem. Int. Ed.* 2013, **52**, 12322-12326, (b) Q. Sun, M. Jiang, Z. Shen, Y. Jin, S. Pan, L. Wang, X. Meng, W. Chen, Y. Ding, J. Li, F.-S. Xiao, *Chem. Commun.* 2014, **50**, 11844-11847, (c) M. Jiang, L. Yan, Y. Ding, Q. Sun, J. Liu, H. Zhu, R. Lin, F. Xiao, Z. Jiang, J. Liu, *J. Mol. Catal. A: Chem.* 2015, **404-405**, 211-217, (d) C. Li, K. Xiong, L. Yan, M. Jiang, X. Song, T. Wang, X. Chen, Z. Zhan, Y. Ding, *Catal. Sci. Technol.* 2016, **6**, 2143-2149, (e) C. Li, K. Sun, W. Wang, L. Yan, X. Su, Y. Wang, K. Xiong, Z. Zhan, Z. Jiang, Y. Ding, *J. Catal.* 2017, **353**, 123-132, (f) T. Wang, Y. Lyu, K. Xiong, W. Wang, H. Zhang, Z. Zhan, Z. Jiang, Y. Ding, *Cuihua Xuebao/Chin. J. Catal.* 2017, **38**, 890-898, (g) T. Iwai, T. Harada, H. Shimada, K. Asano, M. Sawamura, *ACS Catal.* 2017, **7**, 1681-1692, (h) Q. Sun, Z. Dai, X. Meng, F.-S. Xiao, *Chem Mater.* 2017, **29**, 5720-5726.

9 (a) B. Arndtsen, R. Bergman, T. Mobley, T. Peterson, *Acc. Chem. Res.* 1995, **28**, 154-162, (b) H. Davies, J. Manning, *Nature*, 2008, **451**, 417-424, (c) X. Chen, K. Engle, D.-H. Wang, J.-Q. Yu, *Angew. Chem. Int. Ed.* 2009, **48**, 5094-5115, (d) R. Jazzar, J. Hitce, A. Renaudat, J. Sofack-Kreutzer, O. Baudoin, *Chem Eur. J.* 2010, **16**, 2654-2672, (e) M. Chen, C. White, *Science,* 2010, **327**, 566-571, (f) M. Chen, C. White, *Science,* 2010, **318**, 783-787, (g) T. Lyons, M. Sanford, *Chem. Rev.* 2010, **110**, 1147-1169, (h) H. Li, B.-J. Li, *Catal. Sci. Technol.* 2011, **1**, 191-206, (i) G. Rouguet, N. Chatani, *Angew. Chem. Int. Ed.* 2013, **52**, 11726-11743, (j) S.-B. Yan, S. Zhang, W.-L. Duan, *Org. Lett.* 2015, **17**, 2458-2461, (k) J. Hartwig, *J. Am. Chem. Soc. 2016*, **138**, 2-24, (l) G. He, B. Wang, W. Nack, G. Chen, *Acc. Chem. Res.* 2016, **49**, 635-645, (m) J. He, M. Wasa, K. Chan, Q. Shao, J.-Q. Yu, *Chem. Rev.* 2017, **137**, 8754-8786, (n) H.-R. Tong, S. Zheng, X. Li, Z. Deng, H. Wang, G. He, Q. Peng, G. Chen, *ACS Catal.* 2018, **8**, 11502-11512, (o) J. Beck, C. Lacker, L. Chapman, S. Reisman, *Chem. Sci.* 2019, **10**, 2315-2319, (p) S. Rej, Y. Ano, N. Chatani, *Chem. Rev.* 2020, **120**, 1788-1887, (q) O. Shao, K. Wu, Z. Zhuang, J.-Q. Yu, *Acc. Chem. Res.* 2020, **53**, 833-851.

10 (a) Z. Xie, C. Wang, K. deKrafft, W. Lin, *J. Am. Chem. Soc.* 2011, **133**, 2056-2059, (b) J.-L. Wang, C. Wang, K. deKrafft, W. Lin, *ACS Catal.* 2012, **2**, 417-424, (c) W.-J. Yoo, S. Kobayashi, *Green Chem.* 2014, **16**, 2438-2442, (d) M. Liras, M. Pintado-Sierra, M. Iglesias, F. Sánchez, *J. Mater. Chem. A* 2016, **4**, 17274-17278, (e) L. Pan, M.-Y. Xu, L.-J. Feng, Q. Chen, Y.-J. He, B.-H. Han, *Polym. Chem.* 2016, **7**, 2299-2307, (f) L.-C. Lee, J. He, J.-Q. Yu, C. Jones, *ACS Catal.* 2016, **6**, 5245-5250.

11 For recent examples, see: (a) F. Wang, J. Mielby, F Richter, G. Wang, G. Prieto, T. Kasama, C. Weidenthaler, H.-J. Bongard, S. Kegnæs, A. Fürstner, F. Schüth, *Angew. Chem. Int. Ed.* 2014, **53**, 8645-8648, (b) S. Kramer, F. Hejjo, K. Rasmussen, S. Kegnæs, *ACS Catal.* 2018, **8**, 754-759, (c) N. Bennedsen, S. Kramer, J. Mielby, S. Kegnæs, *Catal. Sci. Technol.* 2018, **8**, 2434–2440, (d) J. Huang, M. Hong, C.-C. Wang, S. Kramer, G.-Q. Lin, X.-W. Sun, *J. Org. Chem.* 2018, **83**, 12838-12846, (e) S.

View Article Online
DOI: 10.1039/D0CY01326A

Kramer, *Org. Lett.,* 2019, **21**, 65-69, (f) N. Bennedsen, R. Mortensen, S. Kramer, S. Kegnæs, *J. Catal.* 2019, **371**, 153-160, (g) J. Himmelstrup, M. Buandia, X.-W. Sun, S. Kramer, *Chem. Commun.* 2019, **55**, 12988-12991.

12 A hot filtration experiment was attempted, but unsuccessful due to the extensive swelling of the polymer, which instantly clogs a syringe filter. However, we do believe that observations from a combination of other experiments indicate heterogeneous catalysis: 1) Reaction without (*R*)-P-amidite-POP leads to racemic product (Table 3, entry 2). 2) No ligand leaching could be detected in the liquid phase (Figure S3).

Journal Name ARTICLE

TOC

View Article Online
DOI: 10.1039/D0CY01326A